1up

NASA TECHNICAL MEMORANDUM

NASA TM X-71569

NASA TM X-71569

SPECTROSCOPIC RESULTS IN HELIUM FROM THE NASA LEWIS BUMPY TORUS PLASMA

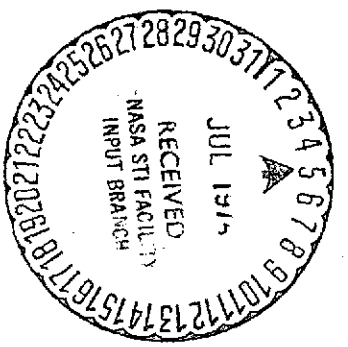

by Richard W. Richardson
Lewis Research Center
Cleveland, Ohio

TECHNICAL PAPER presented at
First International Conference on Plasma Science
sponsored by the Institute of Electrical and Electronics Engineers
Knoxville, Tennessee, May 15-17, 1974

SPECTROSCOPIC RESULTS IN HELIUM FROM THE NASA LEWIS BUMPY TORUS PLASMA

RICHARD W. RICHARDSON*

Lewis Research Center

ABSTRACT

Spectroscopic measurements have been carried out on the NASA Lewis Bumpy Torus experiment in which a steady state ion heating method based on the modified Penning discharge is applied in a bumpy torus confinement geometry. Electron temperatures in pure helium are measured from the ratio of spectral line intensities. Measured electron temperatures range from 10 to 100 eV. Relative electron densities are also measured over the range of operating conditions. Radial profiles of temperature and relative density are measured in the two basic modes of operation of the device called the low and high pressure modes. The electron temperatures are used to estimate particle confinement times based on a steady state particle balance.

E-8006

INTRODUCTION

A hot ion plasma is produced in the NASA Lewis Bumpy Torus confinement geometry by a steady state Penning discharge (ref. 1). The ion heating mechanism associated with the Penning discharge has been explored in a simple magnetic mirror geometry (refs. 2 to 5). It was found that ions with Maxwellian energy distributions and kinetic temperatures as high as several kilovolts could be produced. More recently it has been confirmed that the same mechanism can be used to produce a hot ion plasma in the bumpy torus geometry (ref. 1). To evaluate the possibility of producing a plasma of interest in controlled fusion research with this heating scheme in combination with the confinement geometry it is necessary to obtain information on the plasma density and confinement time and their scaling with operating conditions.

To this end the helium line intensity ratio technique, applicable to this tenuous corona model plasma, has been used to determine electron temperatures over a range of operating conditions. The electron temperatures have then been used with the line intensities to determine the relative electron density. Assuming a steady state discharge the electron temperatures have been used to determine the particle confinement time based on

*NASA-NRC Postdoctoral Research Associate

a simple particle balance. The dependence of these measured and derived quantities on discharge conditions is studied.

APPARATUS AND EXPERIMENTAL PROCEDURE

The NASA Lewis Bumpy Torus magnet facility (refs. 6 and 7) consists of twelve superconducting coils arranged in a toroidal array as shown in figure 1. The major diameter of the torus is 1.52 meters. The 18 cm diameter anode rings at each magnetic mirror midplane are biased to a high positive dc potential relative to the grounded magnet coils and tank wall to produce the discharge. For the spectroscopic measurements to be reported on in this paper the discharge has been operated in pure helium.

The gross voltage and current characteristics for the discharge operating in helium are shown in figure 2 for background helium pressure, p_o, ranging from 0.8 - 18.9×10^{-5} torr and a maximum magnetic flux density of 2.4 tesla. An ion gauge is used to measure background pressure using a gauge factor for helium of 5.55. The discharge operates in two distinct modes as can be seen in figure 2. The mode dominating at low pressures is called the low pressure mode (LPM) and that at high pressures the high pressure mode (HPM). At the lower pressures there is no discontinuity in the I-V curves (no HPM exists) but there is a change in slope of the I-V curve, observed near 10 kV anode voltage.

Electron temperatures and relative electron densities have been determined spectroscopically from line intensities over the range of conditions in figure 2, and over a range of maximum magnetic flux densities of from 0.24 to 2.4 tesla. The spectroscopic measurements were made with a Jarell-Ash 1.5 meter Fastie-Ebert spectrometer with a photomultiplier tube output. Output currents were time integrated with a time constant of several seconds. A thin horizontal chord through the plasma perpendicular to the magnetic flux was viewed through imaging optics as shown in figure 3. The measurements were made at the magnet mirror midplane in the region between a set of double anode rings spaced 3 cm apart. Chords at different vertical positions were observed by translation of the lens perpendicular to the optical axis. A standard lamp was used to determine the spectral response of the entire system. Entrance and exit slits of 100 μ were used for all measurements. With these slit widths no broadening of the spectral lines other than the instrument broadening was observed. For the majority of measurements the plasma was viewed through a fixed chord half way between the edge and center. The spectrum was scanned in the vicinity of the spectral line to allow determination of the baseline and line peak for the intensity measurement.

DETERMINATION OF TEMPERATURE AND DENSITY FROM SPECTRAL INTENSITIES

Electron temperatures are measured by the helium line intensity ratio technique (refs. 8 and 9) for a tenuous corona model plasma. The plasma is assumed to be diffusion dominated with recombination at the walls. This technique utilizes the marked difference in electron energy dependence of the optical cross section of the 4^1S and 5^1S singlet and 4^3S and 5^3S triplet states of neutral helium and between the He^+ $n = 4$ state and the neutral helium states. The emission coefficient of a spectral line ε_{jk} due to a transition $j \rightarrow k$ in the case of single step electron excitation from the ground state and spontaneous decay is

$$\varepsilon_{jk} = n_o n_e \left\langle f_{jk}(v) v \right\rangle \sigma_{jk} = n_o n_e S_{jk}(T_e) \tag{1}$$

where n_o and n_e are the neutral helium and electron number density, respectively, and $S_{jk}(T_e)$ is the excitation rate coefficient. The variable $f_{jk}(v)$ is the apparent optical cross section shape function normalized to its maximum and is a function of the electron velocity v. The angle brackets indicate an average over the assumed electron energy distribution function which is taken to be Maxwellian, and σ_{jk} is the maximum apparent optical cross section. The apparent optical cross sections include cascade from upper states. The ratio of the emission coefficients of two spectral lines, $\varepsilon_{jk}/\varepsilon_{\ell m}$, is independent of electron density and is a function only of electron temperature if the shape functions $f_{jk}(v)$ and $f_{\ell m}(v)$ are dissimilar. The experimental procedure is to form the ratio of two measured relative spectral line emission coefficients $\varepsilon'_{jk}/\varepsilon'_{\ell m}$, where the primes denote measured quantities. The electron temperature is determined to be that for which

$$\frac{S_{jk}(T_e)}{S_{\ell m}(T_e)} = \frac{\varepsilon'_{jk}}{\varepsilon'_{\ell m}}$$

The relative electron density can be determined from the measured electron temperature and a relation of the form

$$n_e \sim \frac{\varepsilon'_{jk}}{n_o S_{jk}(T_e)} \tag{2}$$

This is useful for determining radial density profiles and observing the change in density with operating conditions of the discharge. The conditions under which (1) is expected to describe the population of the n^1S and n^3S states of helium have been discussed by Sovie (ref. 10). Equation (1) can be invalidated by: (1) excitation from metastable states; (2) collisional depopulation of upper excited states at high electron densities; and (3) enhancement of cascade from n^1P to n^1S states due to resonance radiation trapping at high background pressures. The first two cause an underestimate of the electron temperature while (3) causes an overestimate. Consideration of these processes have shown them to be unimportant primarily due to the low neutral background pressures ($0.8 - 18.9\times10^{-5}$ torr).

The excitation coefficients $\sigma_{jk}\left\langle f_{jk}(v)v\right\rangle$ and appropriate ratios as functions of electron temperature have been numerically computed up to an electron temperature of 200 eV for the 2^3P-5^3S (412.1 nm), 2^3P-4^3S (443.8 nm), 2^1P-4^1S (504.8 nm), and 2^1P-5^1S (443.8 nm) transitions of neutral helium. Cross section shape functions used for the singlet states are from references 11 and 12. The shape functions used for the triplet states are those from references 11 and 12 out to an electron energy of 50 eV. The $1/E^3$ electron energy dependence for the triplet state cross section as measured in reference 13 is normalized to those of references 11 and 12 at 50 eV for the higher energies. This results in singlet to triplet rate coefficient ratios which are in agreement with those of reference 9 to about 30 eV but which increase more steeply for electron temperatures above 30 eV. The He^+ 3-4 (468.6 nm) transition excitation coefficient for excitation from the netural ground state has been calculated using the shape functions of references 14 and 15. For all lines the maximum cross sections σ_{jk} of reference 9 were used.

ELECTRON TEMPERATURE AND DENSITY PROFILES

For a set of operating conditions in each mode vertical scans of the plasma were performed for the 504.8 nm and 471.3 nm spectral lines for Abel inversion to radial emission coefficient. The line intensities across a given chord are time averaged with a time constant, T, of up to several seconds determined by the photomultiplier tube output circuitry. The line intensity measured when looking across the plasma at a chord position y up from the axis and at a time t is given by the equation (ref. 16)

$$I_{jk}(y,t) = \int_{-\sqrt{R^2-y^2}}^{\sqrt{R^2-y^2}} n_o n_e(r,\phi,t) S_{jk}\left[T_e(r,\phi,t)\right] d\ell \qquad (3)$$

where $\phi = \sin^{-1}(y/r)$ is an azimuthal angle about the minor axis, d is a length of chord, and R is the minor radius of the torus at the midplane. The possibility of time and azimuthal dependence is included.

A time average of (3) with time constant T is

$$\overline{I_{jk}(y)} = \frac{\int_o^T I_{jk}(y,t)dt}{T} = n_o \int_{-\sqrt{R^2-y^2}}^{\sqrt{R^2-y^2}} \left[\frac{\int_o^T n_e(r,\phi,t) S_{jk}\left[T_e(r,\phi,t)\right] dt}{T} \right] d\ell \qquad (4)$$

where T is determined by the output circuitry of the photomultiplier circuit. In order to apply the Abel inversion it is necessary that the term in brackets (plasma emission coefficient) be independent of ϕ. In this experiment the plasma may be a rotating azimuthal structure, i.e., a spoke, the properties of which are assumed not to be time dependent in the frame of reference of the spoke. This can be incorporated into the time average in (4) by writing the time averaged emission coefficient.

$$\overline{\varepsilon_{jk}(r)} = n_o \overline{n_e S_{jk}(r)} = \frac{n_o \int_o^{\omega_s T} n_e(r,\phi,t) S_{jk}\left[T_e(r,\phi,t)\right] d\omega_s t}{\omega_s T} \qquad (5)$$

where if ω_s is the spoke rotation frequency and if $\omega_s T >> 2\pi$ the time average is an azimuthal average and the resulting emission coefficient is independent of time and azimuth. In figure 4 are shown the time and azimuthally averaged radial plasma emission coefficient profiles $\bar{\varepsilon}(r)$ for the 471.3 nm line for each mode as obtained using the forty point Abel inversion scheme of reference 16. For these two operating modes the background pressure of 8.3×10^{-5} torr was the same and the input powers were 3 kW. Assuming the electron temperature, T_e, is independent of time and azimuthal angle about the minor axis of the torus, the ratio of the time averaged plasma emission coefficients of the singlet and triplet lines at a radial point is a function only of the rate coefficients and therefore electron temperature. Electron temperature radial profiles, $T_e(r)$, in the two modes determined from the 504.8 nm to 471.3 nm intensity ratio are shown in figure 5. Both modes are characterized by an electron temperature which increases near the anode. The time averaged relative plasma density, $\bar{n}_e$, in figure 6 is determined as a function of r for each mode from the temperature profile and the relative emissivity of the

504.8 nm line using equation (2). Figure 6 shows the relative magnitude of the densities for the two modes. In both modes there is a region near the anode in which the densities are comparable. This region will be subsequently referred to as the anode sheath. The HPM electron density is a maximum on the axis of the discharge and for these conditions is nearly an order of magnitude greater than the LPM maximum density. The maximum LPM density occurs near the anode, however, a lower local maximum in density occurs on the axis as shown in figure 6. This is observed visually as is schematically shown in figure 4 as a brighter region near the axis which develops as the input power is increased. At lower input powers this inner bright core of plasma is not observed in the LPM. The radial profiles at the midplane have been used to determine how the plasma fills the discharge volume in the two modes and where particle production occurs. Figure 7 contains a plot of the fraction of particles per unit length contained between r and $R\left(\int_r^R \overline{n_e} r dr \Big/ \int_o^R \overline{n_e} r dr\right)$ for each mode and a plot of the fraction of particles per unit length produced by electron impact ionization between r and $R\left(\int_r^R \overline{n_e} S_i(T_e) r dr \Big/ \int_o^R \overline{n_e} S_i(T_e) r dr\right)$ for each mode. The ionization rate coefficients S_i are determined from reference 17 and the radial electron temperature profiles. In table I are given in relative units the denominators of these two expressions representing the relative number of particles per unit length and relative number of particles produced per unit length for each mode. It is evident from figure 7 that in the LPM most of the plasma and plasma production occurs in or near the sheath. Since the LPM plasma is not observed to completely fill the plasma volume away from the midplane (defined by magnetic field lines which intersect the anode ring) it is expected that the plasma and its production primarily occurs in the anode sheath. In the HPM the bulk of the plasma is in the center of the discharge as is shown in figures 6 and 7. Production of plasma in the HPM anode sheath is enhanced by the higher temperature. However, due to the lower density relative to the center this extra production amounts to only about 20 percent more than would occur if the sheath temperature were uniform and equal to that in the bulk of the plasma. The HPM plasma boundary is visually observed to follow the magnetic flux lines intersecting the anode very sharply, filling the discharge volume away from the midplane where the anode sheath will not contribute to plasma production. The actual contribution of the sheath to total plasma production is then expected to be less than the 20 percent calculated for the midplane, probably less than 10 percent of the total considering the relative volumes of plasma and

sheath. This analysis of the radial profiles and visual appearance of the plasma leads to the qualitative conclusion that the LPM is dominated by processes in the anode sheath whereas the HPM is dominated by processes in the entire discharge volume. The ratio of the particle production per unit length to the number of particles per unit length, which is the mean electron ionization rate $\bar{S}_i$, is also shown in table I along with the mean electron temperature $\bar{T}_e$ corresponding to $\bar{S}_i$. Reference to figures 5 and 6 indicates that the mean electron temperature is characteristic of the bulk of the plasma for the HPM.

The inverse of $n_o\bar{S}_i$, where n_o is the neutral density, is the mean ionization time τ_i and is shown for each mode in table I. The mean ionization time is a factor of three longer for the HPM than the LPM at similar operating conditions (neutral density and input power). For the time averaged corona model plasma used here this mean ionization time should be equal to the mean particle containment time, τ_p (the ion charge containment time), assuming no other production processes are important.

T AND n FROM CHORD AVERAGES

Due to the long time required to take vertical scans for Abel inversion to radial profiles, these scans were taken at only a few representative conditions. Line intensities from time and hence azimuthally averaged plasma emissivities spatially averaged across a single chord were used to determine plasma electron density and electron temperature over a wider range of operating conditions. A chord at vertical position $y = R/2$ halfway between the edge and axis of the discharge was viewed. Equation (4) describes the time averaged chordwise line intensity observed in terms of the local emission coefficient.

In the case of the HPM reference to the radial profiles of the previous section and the line excitation functions allows an estimate of relative amounts of light collected from the sheath and plasma region. Due to the shorter length of chord passing through the sheath region than through the plasma region, and the lower density in the sheath the higher temperature in the sheath accounts for less than 5 percent of the light collected across the chord. The radial dependence of the temperature then occurs where the contribution to the chord integral in equation (4) is small and the radial dependence can be neglected. The ratio of emission coefficients averaged across a chord can then be used to determine the electron temperature, T_e.

For the case of the LPM the radial temperature dependence cannot be handled so easily since reference to the radial profiles and excitation functions shows that light is collected mostly from the sheath region where

the radial temperature dependence is most pronounced. It is necessary to resort to comparison of the chord average temperature to the temperature determined from the radial profile. The temperature as determined from a chordwise intensity ratio at $y = R/2$ for the LPM considered in the previous section gives an electron temperature of 40 eV representative of the electron temperature at the peak of the sheath density. This compares closely with the temperature of 45 eV in table I determined from the mean ionization rate.

The intensities of the 504.8 ($4^1S - 2^1P$), 443.8 ($5^1S - 2^1P$), 471.3 ($4^3S - 2^3P$), 412.1 ($5^3S - 2^3P$), and 468.6 (He II 4-3) spectral lines were measured at each set of operating conditions. Electron temperatures were determined from all possible singlet to triplet and neutral helium to He^+ chordwise line intensity ratios. A statistical analysis of temperature ratios such as $(T_{504.8/471.3}/T_{443.8/412.1})$ for all sets of conditions indicated an agreement between the four temperatures from the singlet and triplet ratio of better than 10 percent with a standard deviation of 10 percent over all data sets. Electron temperature measured from the He^+ and neutral helium ratios read a consistent 10 eV high for all conditions, corresponding to a factor of two high at low temperatures to 10 percent at high temperatures. This trend also held for the radial profile data, indicating that the disagreement did not result from the higher electron temperature near the edge. It is believed that the high He^+ line intensity resulting in the high temperature is due to an enhanced tail on the electron energy distribution function or direct excitation of helium ions. The electron temperature to be presented resulted from the average of the electron temperature as determined from each of the singlet and triplet ratios, and does not include the temperature determined from the He^+ line.

Chordwise averaged relative electron densities $\bar{\bar{n}}_e = I'_{jk}/n_o S_{jk}(T_e) \sim \int \bar{n}_e(r)d\ell$, where I'_{jk} is the measured intensity, were determined for each of the four spectral line intensities using the averaged electron temperature. The average of the four densities is used.

Electron temperatures and relative electron densities were measured for the LPM and HPM for a background pressure, p_o, range of 0.8 to 18.9×10^{-5} torr, an anode voltage range of 2.5 to 27.5 kV with input power ranging from 13 watts to 54 kW. The majority of the data were taken with a maximum magnetic flux density of 2.4 tesla. Electron temperatures measured for the HPM ranged between 10 and 30 eV, while those for the LPM ranged between 30 and 100 eV. In figure 8 are plotted curves of electron

temperatures versus anode voltage for several background pressures. The data at 3.9, 1.5, 0.78×10^{-5} torr were entirely in the LPM. A change in the trend of electron temperature versus voltage is observed to occur at about 10 kV, corresponding to the point at which a slight change in slope can be seen on the I-V plots of figure 2. At anode voltages of 15 kV and higher, the temperatures in the LPM decrease as the pressure is lowered. At $p_o = 15.5\times10^{-5}$ torr all data were in the HPM. The data at 6.1×10^{-5} torr show the effect of the mode change on the electron temperature. The data at the other pressures for the two modes follow these same trends. Electron temperatures were also measured at a fixed anode voltage of 20 kV and a background pressure of 5.5×10^{-5} torr in the LPM for maximum magnetic field densities ranging from 0.24 to 2.4 tesla. The temperature was observed to be 80 eV ± 5 eV over the range of magnetic flux density with no systematic trend evident. Gross discharge characteristics were also insensitive to magnetic flux density. This indicates that the observed electron temperatures do not result from direct ExB heating, since the electron energy would be expected to have a strong inverse squared dependence on magnetic flux density (ref. 18).

The chord averaged density data as a function of anode current are shown in figure 9. Data points at a given pressure are connected to clarify the observed trend. In general the density increases as the square root of the current. This dependence is the same as was determined in a helium seeded deuterium plasma reported previously (ref. 1). A saturation of the density is observed in the HPM at the higher currents. This may be related to excessive heating of the anode support structure which occurs under these conditions. At a given discharge current the electron density is observed to increase with decreasing background pressure.

Mean electron ionization times have been calculated from the chord averaged electron temperature and the relation $\tau_i = \left[n_o S_i(T_e)\right]^{-1}$ where the electron impact ionization rate coefficients, $S_i(T_e)$, are taken from reference 17 and n_o is the neutral background density. The resulting times are plotted in figure 10 as a function of electron temperature with background pressure as a parameter. For the steady state plasma model used here the mean electron ionization time can be identified with the particle confinement time, τ_p, assuming no other ionization processes are important. The confinement time ranged between 15 and 250 μsec. At a given pressure the particle confinement time is much less in the LPM than in the HPM. Although it cannot readily be seen from figure 10, the confinement times were found to be inversely proportional to the background pressure at a given anode voltage. The result that the electron temperature is constant with magnetic flux density for the LPM leads to the

result that the confinement time is independent of magnetic flux density at least in the LPM.

The quantity $\bar{\bar{n}}_e/\tau_i$ has been calculated for the various operating conditions and is plotted versus the discharge current, I, in figure 11 for the LPM. The LPM mode data have been found to fall into two groups. One group is denoted by the square symbol in figure 11 and corresponds to data below the change in slope of the V-I curves for the LPM on figure 2. The other group corresponding to the circular symbol are for data taken above the change in slope of the V-I curves. There is an electron density boundary between these two groups; the electron density being low for the points below the change in slope and high for points above the change in slope. The latter group of data fall along a straight line at 45° over the range of conditions indicating that $I \propto \bar{\bar{n}}_e \tau_i^{-1}$. The data from the first group diverge from the 45°. For a steady state plasma the dependence $I \propto \bar{\bar{n}}_e/\tau_i$ is consistent with an expression which has been suggested for the discharge current in (ref. 18),

$$I = \hat{n}_e/\tau_p \; eVp \tag{6}$$

where Vp is the plasma volume and $\hat{n}_e = \bar{n}_e \, dVp/Vp$, i.e., the mean plasma density averaged over the entire plasma volume. This expression is valid if the anode collects only electrons and the cathode (all other surfaces) collect only ions. This possibility has been suggested since electrons cannot easily cross the strong magnetic flux lines at the cathode so that the current may be completed by the ions which have a higher cross field mobility. Equation (6) can in principle be used to estimate the density $\hat{n}_e$. However, consideration of the radial profiles indicated the azimuthally averaged plasma is localized near the anode sheath. The spoke picture suggests the plasma is also localized azimuthally in the sheath region. Use of a plasma volume of 82×10^3 cm^3 as defined by the magnetic flux line anode ring intersection predicts a maximum spatially averaged density of 2×10^9 cm^3. This probably underestimates the local plasma electron density by a factor of the ratio of the magnetic flux defined volume to the actual local plasma volume which could be significantly smaller but cannot at this time be estimated. In figure 12 is plotted a curve of n_e/τ_i versus I for the HPM. A definite trend is evident; however, it does not agree as well with the simple picture of equation (6), and a more complicated model of the plasma is required.

In figure 13 the quantity $\bar{n}_e T_i/\tau_i$ has been plotted as a function of the input power, P, where T_i is the ion temperature determined from charge exchange neutral data (unpublished). Data are plotted only for the LPM points above the change in slope on figure 3. Ion temperatures were not measurable either below the change in slope of the LPM or for any of the HPM when running pure helium. These data also indicate a dependence of the form $P \propto \bar{n}_e T_i/\tau_i$ indicating that the energy loss time τ_E is equal to or at least proportional to the mean particle loss time.

SUMMARY AND CONCLUSIONS

The radial structure of the two modes of operation of the discharge, the LPM and HPM, have been studied in helium gas at the magnetic mirror midplane from spectroscopically determined radial profiles of electron temperature and densities. The conclusion has been drawn that the LPM plasma and production processes are localized near the anode and the plasma does not fill the discharge volume . On the other hand the HPM fills the discharge volume defined by the intersection of the magnetic flux lines with the anode and plasma production occurs throughout the volume. The precise mechanism of this mode change has not yet been determined.

The major result of this work has been the determination of the dependence of the relative electron density and confinement time on operating parameters. It has been shown that for the LPM $I \propto \hat{n}_e/\tau_p$ consistent with the model in which only electrons go to the anode and only ions go to all other surfaces (cathode). This indicates that ambipolar diffusion is not important in this mode. Of interest is the result that the particle confinement time, τ_p, for the LPM is independent of magnetic flux density and inversely proportional to the discharge pressure at a given discharge voltage. These dependences are consistent with predictions for neoclassical collisionless diffusion in a bumpy torus (ref. 19). However, this may be fortuitous since it is not clear that the collisionless regime of the neoclassical theory describe this experiment. The relation (6) has been used to estimate the absolute electron density. This is not expected to give a reliable estimate since the appropriate plasma volume Vp is unknown.

REFERENCES

1. J. R. Roth, R. W. Richardson, and G. A. Glenn, "Initial Results from the NASA Lewis Bumpy Torus Experiment," National Aeronautics and Space Administration, Tech. Memo. TM X-71468, Aug. - Nov. 1973.

2. J. R. Roth, "Experimental Study of Spectral Index, Mode Coupling, and Energy Cascading in a Turbulent, Hot-Ion Plasma," Phys. Fluids, vol. 14, pp. 2193-2202, Oct. 1971.

3. J. R. Roth, "Origin of Hot Ions Observed in a Modified Penning Discharge," Phys. Fluids, vol. 16, pp. 231-236, Feb. 1973.

4. J. R. Roth, "Hot Ion Production in a Modified Penning Discharge," IEEE Trans. Plasma Sci., vol. 1, pp. 34-45, Mar. 1973.

5. J. R. Roth, "Energy Distribution Functions of Kilovolt Ions in a Modified Penning Discharge," Plasma Phys., vol. 15, pp. 995-1005, Oct. 1973.

6. J. R. Roth, A. D. Holmes, T. A. Keller, and W. M. Krawczonek, "Characteristics and Performance of a 12-Coil Superconducting "Bumpy Torus" Magnet Facility for Plasma Research," National Aeronautics and Space Administration, Tech. Note TN D-7353, Aug. 1973.

7. J. R. Roth, A. D. Holmes, T. A. Keller, and W. M. Krawczonek, "A 12-Coil Superconducting "Bumpy Torus" Magnet Facility for Plasma Research," in IEEE Proc. 1972 Applied Superconductivity Conf., pp. 361-366, May 1972.

8. R. J. Sovie, "Spectroscopic Determination of Electron Temperature and Percentage Ionization in a Helium Plasma," Phys. Fluids, vol. 7, pp. 613-614, Apr. 1964.

9. I. D. Latimer, J. I. Mills, and R. A. Day, "Refinements in the Helium Line Ratio Technique for Electron Temperature Measurement and Its Application to the Precursor," J. Quant. Spectr. Rad. Trans., vol. 10, pp. 629-635, 1970.

10. R. J. Sovie, "The Effects of Cascading and Metastable Atoms on the Determination of Electron Temperature from Relative Line Intensities in a Tenuous Helium Plasma," J. Quant. Spec. Rad. Transf., vol. 8, pp. 833-838, 1968.

11. J. D. Jobe and R. M. St. John, "Absolute Measurements of the 2^1P and 2^3P Electron Excitation Cross Sections of Helium Atoms," Phys. Rev., vol. 164, pp. 119-121, Dec. 5, 1967.

12. I. D. Latimer, private communication.

13. R. B. Kay and J. G. Showalter, "Exchange Excitation in Helium: Excitation Functions for the 4^3S, 3^3P, and 3^3D Levels," Phys. Rev. A., vol. 3, pp. 1998-2006, June 1971.

14. R. M. St. John and C. C. Lin, "Production of Excitation and Ionization in Helium by Single Electron Impact," J. Chem. Phys., vol. 41, pp. 195-197, July 1, 1964.

15. H. R. M. Moussa, "Excitation of Helium to Excited Ion States by Electron and Proton Impact," Physica, vol. 36, pp. 646-654, 1967.

16. W. Lochte-Holtgreven, ed., Plasma Diagnostics. Amsterdam: North Holland Publishing Co., 1968, pp. 184-186.

17. W. Lotz, "Electron-Impact Ionization Cross-Sections and Ionization Rate Coefficients for Atoms and Ions from Hydrogen to Calcium," Zeit. fur Phys., vol. 216, pp. 241-247, 1968.

18. J. R. Roth, "Ion Heating Mechanism in a Modified Penning Discharge," National Aeronautics and Space Administration, Tech. Note TN D-6985, Sept. 1972.

19. L. M. Kovrizhnykh, "Transport Phenomena in Toroidal Magnetic Systems," Soviet Phys.-JETP, vol. 29, pp. 475-482, Sept. 1969.

TABLE I. - RESULTS FROM RADIAL PROFILE INTEGRATIONS

	HPM	LPM
$I_1 = \int_0^R \bar{n} r\, dr$, ARB UNITS	2.5×10^5	6.9×10^4
$I_2 = \int_0^R \bar{n} \bar{S}_i r\, dr$, ARB UNITS	9.3×10^{-4}	8.2×10^{-4}
$\bar{S}_i = I_2/I_1$, CM^3/SEC	3.7×10^{-9}	11.9×10^{-9}
$\bar{\tau}_i = (n_0 \bar{S}_i)^{-1}$, μSEC	92	28
$\bar{T}_e$ FROM $\bar{S}_i$, eV	18	45

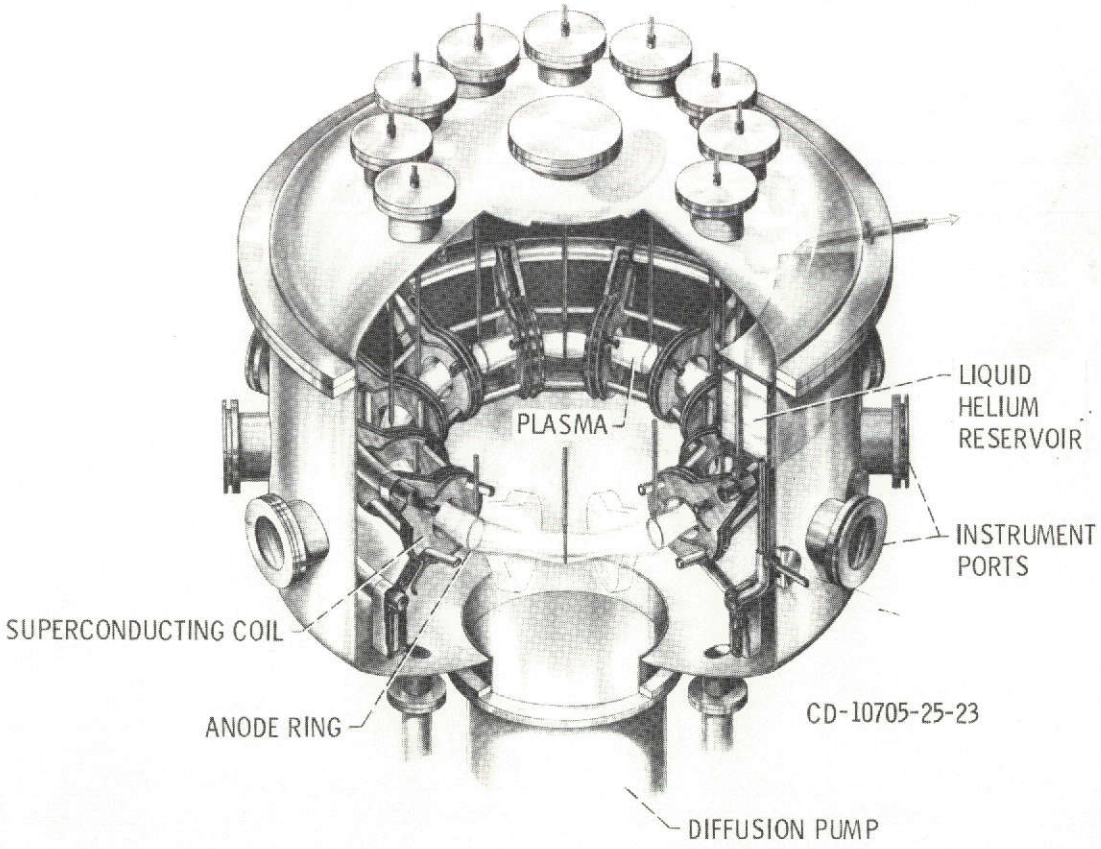

Figure 1. - Schematic of bumpy torus magnetic confinement geometry.

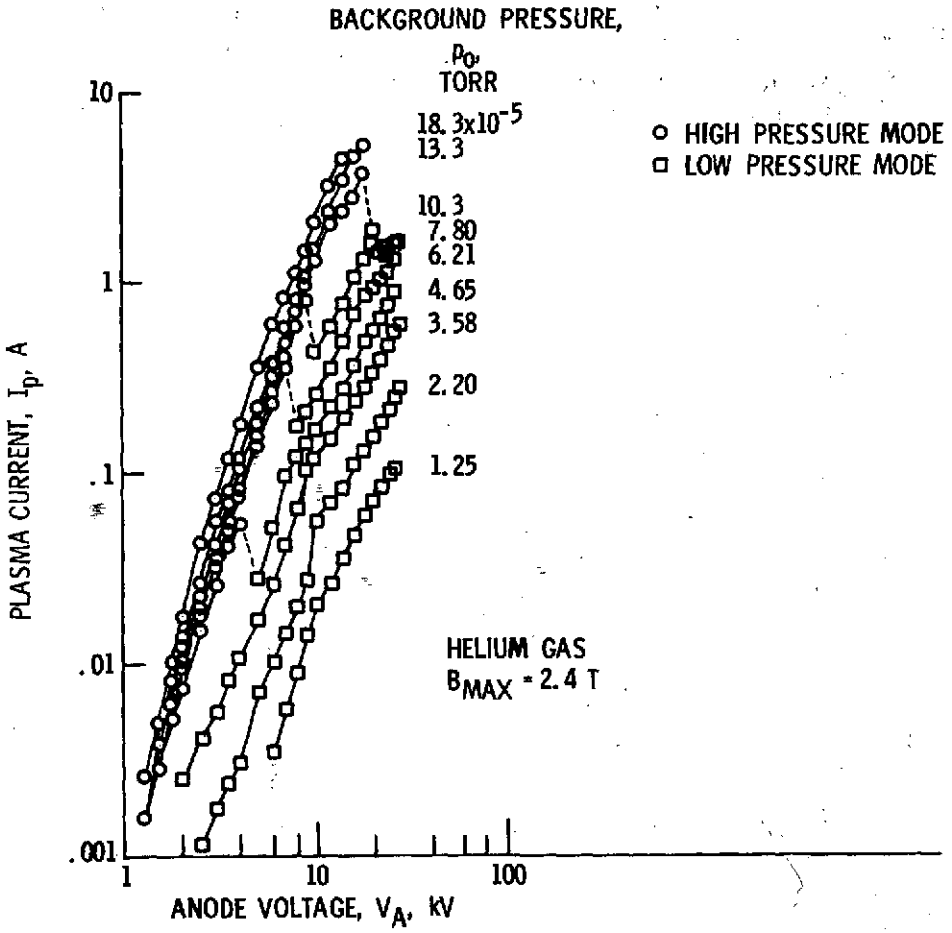

Figure 2. - Voltage-current characteristics for discharge operating in pure helium at B_{max} = 2.4 tesla.

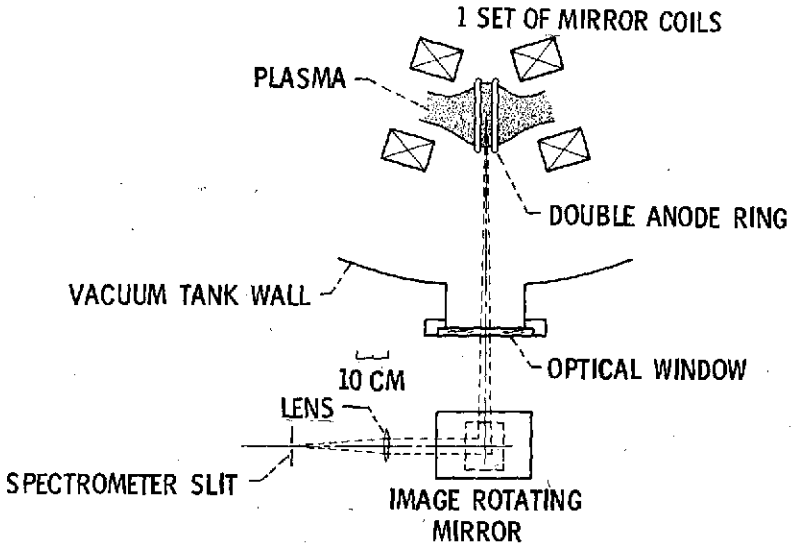

Figure 3. - Schematic drawing of the spectroscopic apparatus used to take electron temperature, relative electron number density, and radial profiles of these quantities.

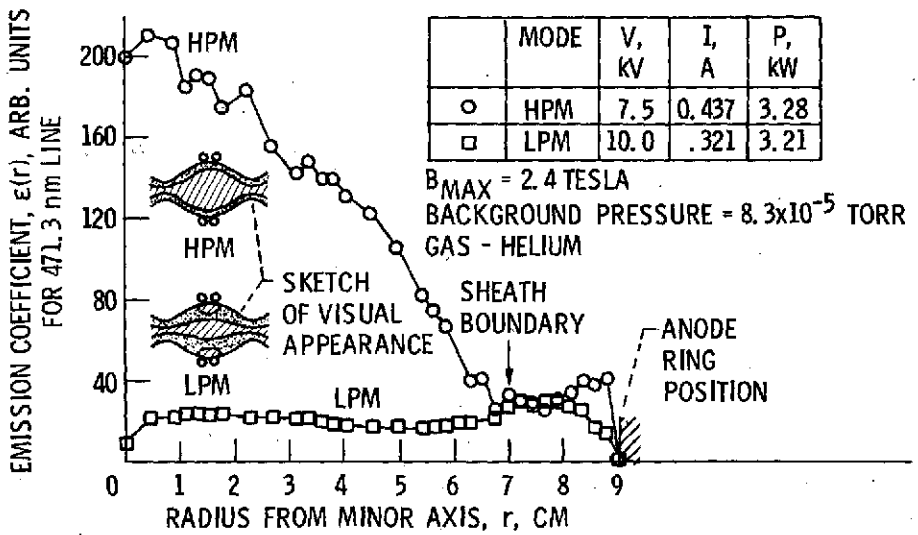

Figure 4. - Plasma emission coefficient radial profile for 471.3 nm spectral line for the two operating modes.

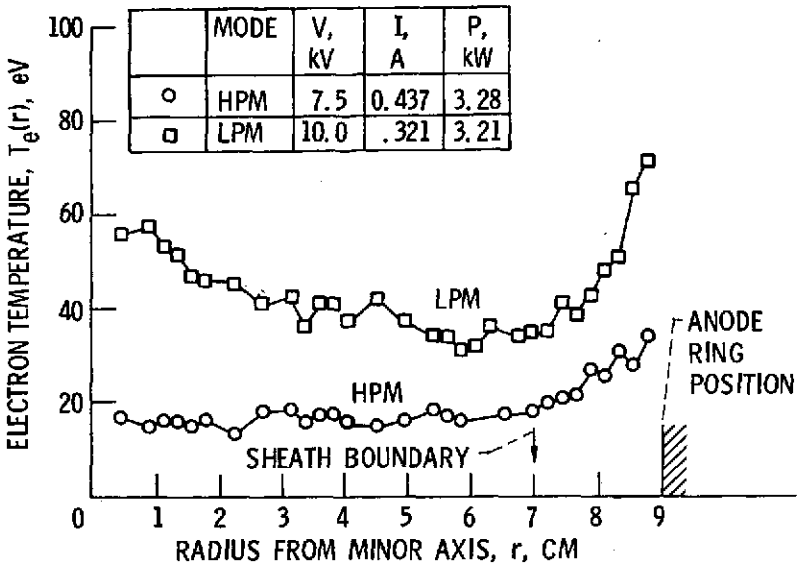

Figure 5. - Plasma electron temperature radial profiles as determined from ratio of 504.8 and 471.3 nm line emission coefficients.

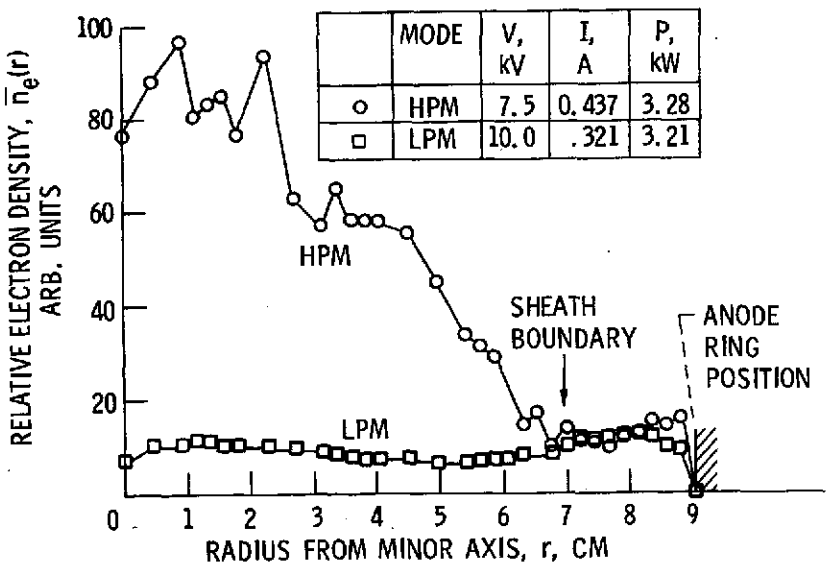

Figure 6. - Radial profiles of relative electron density from emission coefficient of 504.8 nm line and electron temperature from figure 5.

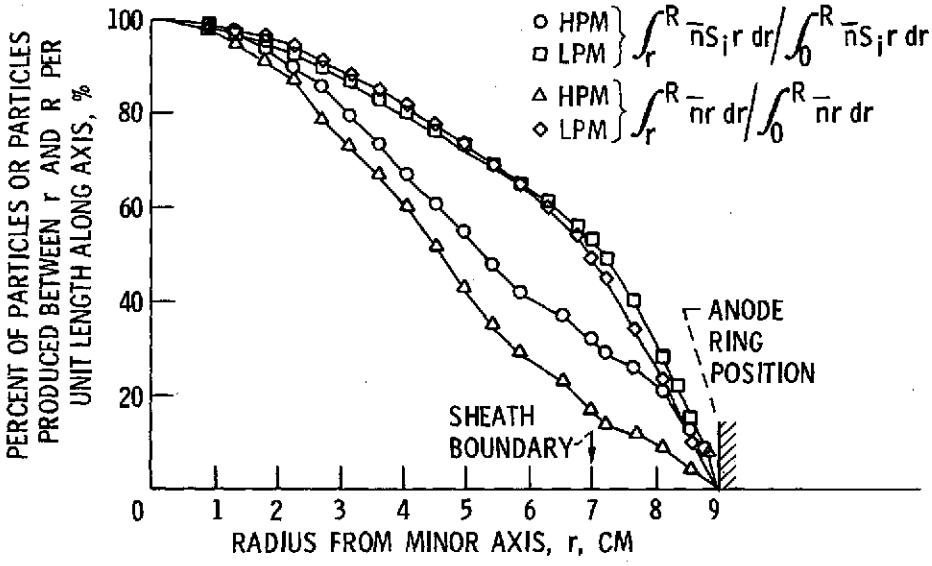

Figure 7. - Plots showing normalized integrations from r→R as a function of r of number of particles and particle production rate per unit length at the magnetic field midplane.

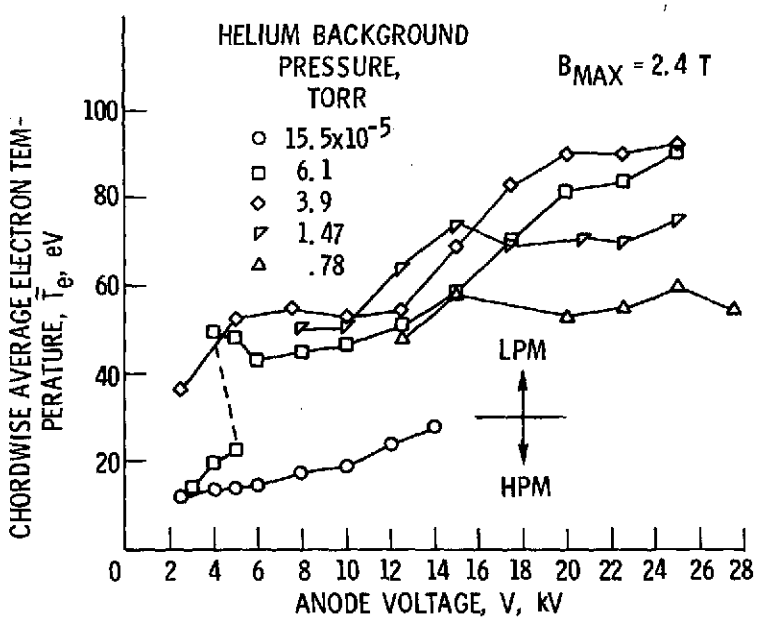

Figure 8. - Chord averaged electron temperature, $\bar{T}_e$, plotted versus anode voltage with background pressure as a parameter.

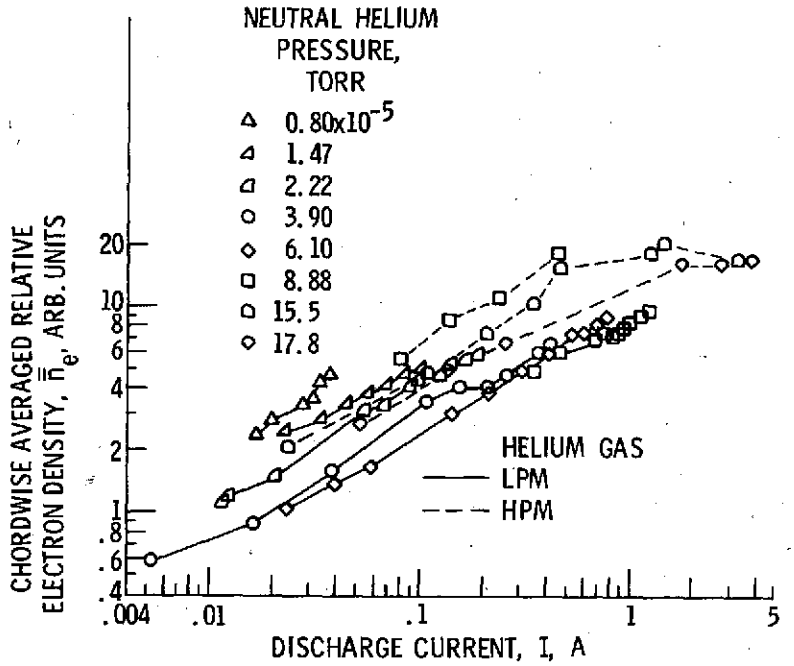

Figure 9. - Relative electron density as a function of discharge current for various background pressures in the two modes.

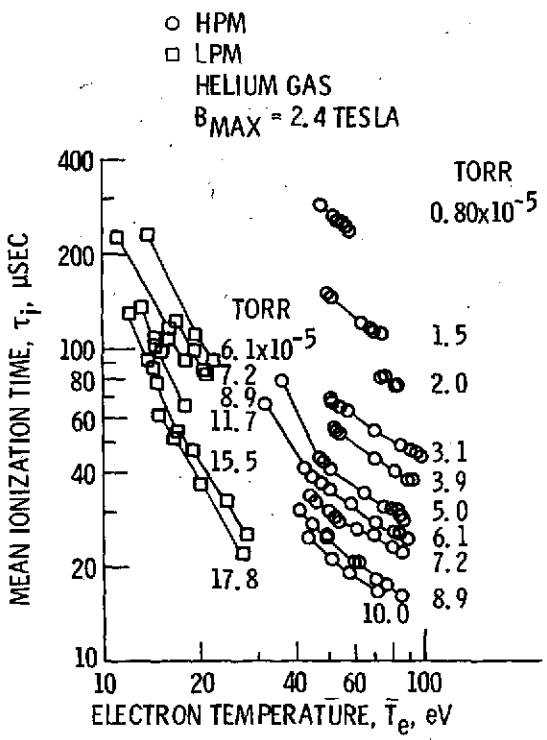

Figure 10. - Mean ionization τ_i for different operating pressures from spectroscopic temperature T_e.

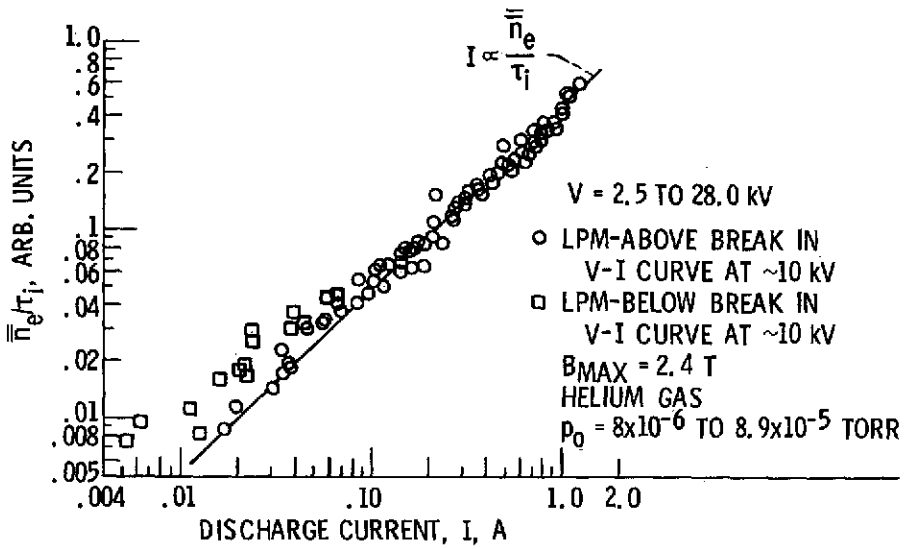

Figure 11. - Characteristic dependence of $\bar{\bar{n}}_e/\bar{\tau}_i$ on discharge current for LPM where τ_i is mean ionization time in μsec.

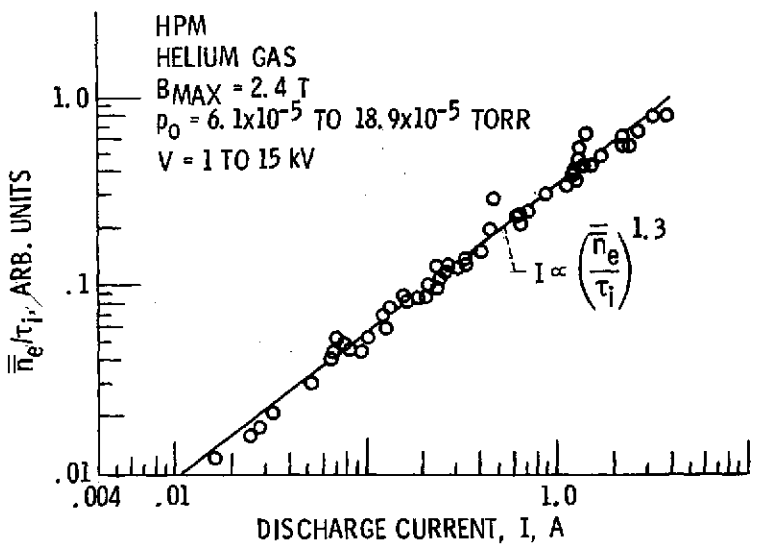

Figure 12. - Characteristic dependence of $\bar{\bar{n}}_e/\bar{\tau}_i$ on discharge current for HPM.

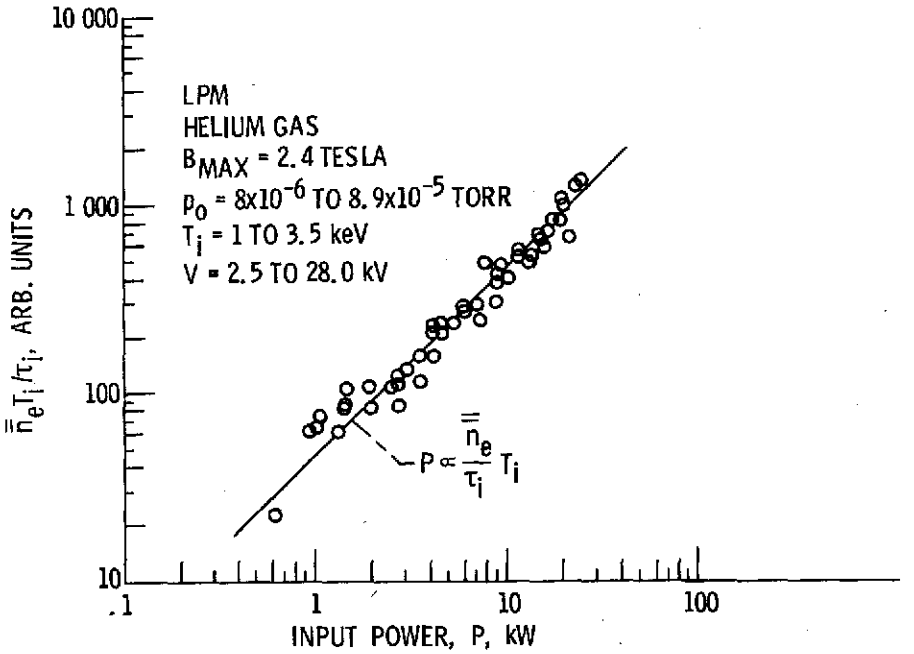

Figure 13. - Characteristic dependence of $\bar{\bar{n}}_e T_i / \bar{\tau}_i$ on discharge input power. T_i is the ion temperature determined from charge exchange neutral data; τ_i is the mean ionization time in μsec.